理學碩士 學位論文

Synthesis and Photophysical Properties of Diboron Multi-Resonance Fluorescent Emitters Incorporated with Polycyclic Aromatic Hydrocarbons

(다환 방향족 탄화수소기가 도입된 이중보론계 다중공명 형광체의 합성 및 광물리적 특성 연구)

蔚 山 大 學 校 大 學 院

化 學 科

韓 昇 希

Synthesis and Photophysical Properties of Diboron Multi-Resonance Fluorescent Emitters Incorporated with Polycyclic Aromatic Hydrocarbons

(다환 방향족 탄화수소기가 도입된 이중보론계 다중공명 형광체의 합성 및 광물리적 특성 연구)

指 導 敎 授 이 민 형

이 論文을 理學碩士 學位 論文으로 제출함

2024年 02月

蔚 山 大 學 校 大 學 院

化 學 科

韓 昇 希

韓昇希의 理學碩士 學位 論文을 認准함.

審査委員 우 상 국 印

審査委員 이 민 형 印

審査委員 정 재 훈 印

蔚 山 大 學 校 大 學 院

2024年 02月

Synthesis and Photophysical Properties of Diboron Multi-Resonance Fluorescent Emitters Incorporated with Polycyclic Aromatic Hydrocarbons

Abstract

Recently, there have been developments in the field of organic light-emitting diode (OLED) devices that utilize DABNA-based multi resonance thermally activated delayed fluorescence (MR-TADF) emitters, which exhibit high efficiency and color purity. However, MR-TADF emitters tend to have long-lived T_1 excitons, which can lead to severe chemical degradation processes initiated in the triplet state. To address these drawbacks and improve the longevity and color purity of OLED devices, it is crucial to develop emitters that do not undergo delayed fluorescence. In this study, we synthesized Xyl-diOBN-Pyr(1) and Xyl-diOBN-Ph-ant(2) compounds by introducing Polycyclic Aromatic Hydrocarbons (PAHs) with low triplet energy into the DABNA skeleton, thereby inducing a low T_1 energy. This modification facilitates the preventing of Dexter energy transfer and promotes the non-radiative decay of the triplet state, ultimately preventing device degradation originating from the triplet excited state. All compounds exhibited normal fluorescence in the deep blue region (455, 450 nm) with high PLQY ranging from 74% to 99% in toluene solutions. These compounds also displayed a large $\triangle E_{ST}$(0.70, 0.99 eV) due to their low T_1 energy. Notably, they exhibited high thermal stability with decomposition temperatures exceeding 461 °C. The details of synthesis and photophysical properties of compounds will be discussed with theoretical study.

국문초록

최근 높은 효율과 고색순도를 보이는 DABNA 형태의 다중 공명 열활성지연형광체를 최종 형광체로 활용하는 초형광 OLED 소자가 개발되고 있다. 하지만, 다중 공명 열활성지연형광체는 긴 삼중항 수명을 갖기 때문에 삼중항 상태에서 유발되는 심각한 화학적 분해과정을 겪게 된다. 이러한 단점을 개선하고 OLED 소자의 수명과 색순도를 향상시키기 위해 지연형광이 일어나지 않는 발광체의 개발이 필요하다. 본 연구에서는 이중보론계 DABNA 골격에 낮은 삼중항 에너지를 가지는 다환 방향족 탄화수소를 도입함으로써 낮은 삼중항 들뜬 상태(T_1) 에너지를 유도하고 이로부터 Dexter 에너지 전달 방지와 삼중항의 비발산성 붕괴를 촉진시킴으로써 삼중항 들뜬상태에서 기인하는 소자 열화를 방지하는 Xyl-diOBN-Pyr(1), Xyl-diOBN-Ph-ant(2) 화합물을 합성하였다. 두 화합물은 톨루엔 용액에서 74%-99%의 높은 PLQY를 가지며 진한 파란색 영역(455 nm, 450 nm)에서 정상적인 형광을 나타내며 낮은 삼중항 에너지로 인해 큰 $\triangle E_{ST}$를 나타낸다(0.70 eV, 0.99 eV). 특히 461 ℃ 이상의 높은 열분해 온도를 통해 높은 열적 안정성이 관찰되었다. 화합물의 합성 및 광물리학적 특성에 대한 자세한 내용은 이론적 연구와 함께 논의된다.

Contents

List of Figures

List of Schemes

List of Tables

I. Introduction

1. Organic Light Emitting Diodes (OLEDs)

Organic light emitting diodes (OLEDs) are 'self-emissive displays' that utilize organic materials to emit light when an electric current flows through them. Unlike liquid crystal displays (LCDs), which use a backlight source along with liquid crystals and color filters to represent colors, OLED displays represent colors through RGB emissive materials that react to the current when applied to the organic emitting layer. Each individual pixel emits its own light, making OLED displays excellent in terms of image quality, thickness, and power efficiency. Furthermore, their flexible allows them to be bent and folded, making them suitable for a wide range of applications. Taking a closer look at these advantages, OLED's rapid electron mobility and its characteristic of being current driven without the need for liquid crystals allow it to achieve a swift response time. As a result, it can display fast and natural movements without noticeable delays. In contrast to LCDs, which require a constant backlight, OLED only illuminates the necessary pixels, significantly reducing power consumption when displaying darker images. Additionally, its structural simplicity, compared to LCDs, results in a thinner and lighter design, approximately 30% thinner.[1,2] A thinner panel not only allows for slimmer product designs but also optimizes the environment for mobile devices by providing more space for batteries. Flexible OLED, utilizing flexible Polyimide (PI) substrates and thin-film encapsulation technology, creates bendable panels. Unlike the challenging processing of glass, PI substrates can be made much thinner, further reducing the overall weight. Furthermore, the introduction of foldable OLED and expandable slider OLED has brought about mobility innovation, enhancing convenience for users of large-screen devices. These designs, which allow for folding and unfolding, contribute to the evolution of mobility. The first component that can be called OLED was invented by Dr. Ching W. Tang and Dr. Steven Van Slyke in 1987 during their research on solar cells at Kodak in the United States. In 1990, a Polymer light-emitting was invented at the Cavendish Laboratory, University of Cambridge in the United Kingdom. Japanese electronics companies also developed oxide Thin-Film Transistor (TFT) technology based on this component.[1,17] They attempted to commercialize large OLED display devices for a long time but faced significant technical challenges, which led to a focus on LCD technology instead. Some of the challenges include the fact that the screen brightness of OLED products is dimmer compared to LCD products.[3] OLED has the characteristic that as the

component produces brighter light and receives more heat, its lifetime decreases. Therefore, OLED products are set with lower average and maximum brightness levels compared to LCD products, even though they can produce brighter screens. Additionally, from a price perspective, OLED is more expensive than LCD. To overcome these challenges, ongoing research is being conducted for the commercialization of OLED technology.[4] Therefore, there is a continuous need for research to improve the efficiency, lifetime, and light output of OLED devices.[3] It's also crucial to lower the operating voltage to increase power conversion efficiency.

2. Multi-layer OLEDs

The typical structure of an OLED consists of a transparent Indium Tin Oxide (ITO) anode layer on a substrate, such as glass, with multiple organic thin films that have varying charge transport capabilities, and an Mg-Ag alloy cathode formed sequentially.[4] Starting from the anode side, these thin films include a hole injecting layer (HIL) containing metal complexes, a hole transport layer (HTL), an emitting layer (EML), and an electron transport layer (ETL), with the organic thin film having a thickness of about 100 nm.[9,17] The cathode is used to allow light generated in the emitting layer to exit and typically utilizes a transparent electrode like ITO. Since OLED is a charge-injection luminescent device, the charge injection efficiency between each interface is the most significant factor affecting the device's performance. Additionally, a hole injection layer (PEDOT: PSS or Cu-PC) is added between the anode and the hole transport layer to reduce the energy barrier for hole injection, and an electron injection layer (0.5–1 nm thick) containing materials like LiF, LiO, CsF is inserted between the cathode and the electron transport layer to enhance electron injection, thereby improving light emission efficiency.[4,8,9] The hole transport layer employs electron-accepting molecules to facilitate easy hole injection from the anode and is primarily composed of electron-donating components based on a basic structure like triphenylamine, diamine, triamine, or tetraamine derivatives. The emitting layer produces light by recombining injected electrons and holes, with the emitted light's color depending on the combination of materials used in the emitting layer.[4] The electron transport layer needs to have high electron mobility to efficiently transport electrons to the emitting layer and prevent unrecombined holes from reaching the cathode, thereby increasing the chances of exciton recombination in the emitting layer.[5,6,7] It should exhibit good electron affinity and adhesion to the cathode electrode.

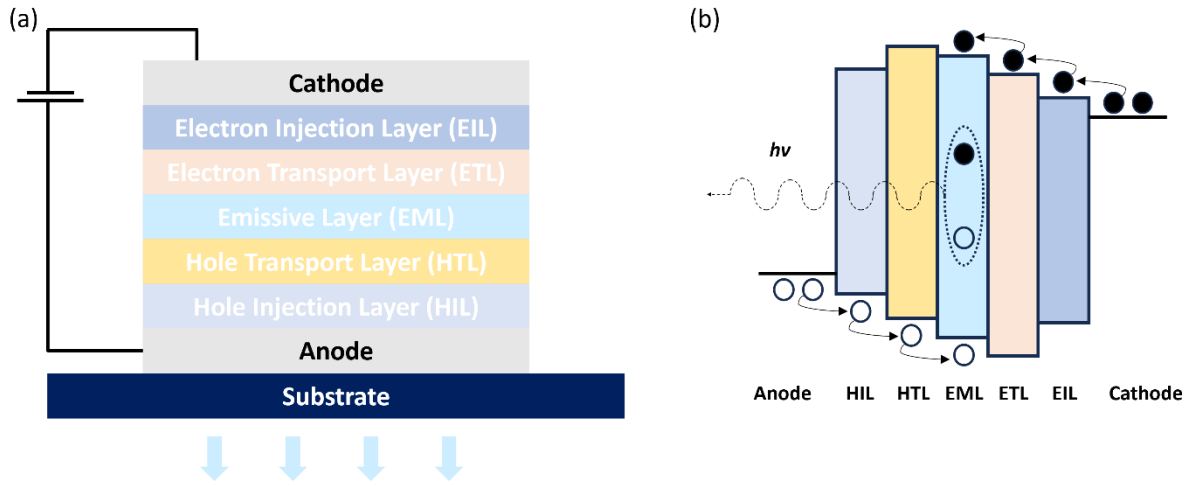

Figure 1. (a) Multi-layer OLEDs structure, (b) Flow of electrons and holes[7]

3. Working Principle of OLEDs

When a voltage is applied between the two electrodes, positive charges (holes) are injected from the anode, and negative charges (electrons) are injected from the cathode.[4,7] They travel through the respective hole transport and electron transport layers to reach the emitting layer. Once there, electrons and holes meet and from excitons. Light is emitted because of the recombination of these excitons, and they return to their ground state. The wavelength of the emitted light is determined by the energy of the exciton, specifically the energy difference between the highest occupied molecular orbital (HOMO) and the lowest unoccupied molecular orbital (LUMO).[17] This generated light is emitted toward the transparent electrode. Examining the detailed mechanism of luminescence, the injection of carriers occurs at the organic layers from both electrodes. These carriers travel through the device, with electrons moving along the conduction path from the cathode and holes moving along the valence band from the anode. The injected electrons and holes within the emitting layer interact through electron-lattice interactions to generate negative and positive polarons. These generated polarons move along the molecular chains under the influence of an applied electric field within the organic material. These mobile polarons encounter and recombine at a specific point within the emitting material to form a singlet polaron exciton. When these excitons deactivate within the emitting material, light is produced corresponding to the energy difference between the polaron and exciton. When singlet excitons are formed, they lead to fluorescence, as they transition to the ground state. However, in the process, when singlet excitons are formed, they occur at a 3:1 ratio with

triplet excitons. In typical organic materials, triplet excitons do not lead to luminescence, following quantum mechanical selection rules. Theoretical internal quantum efficiency (IQE) of OLED devices can reach a maximum of 25%.[4] Triplet excitons can be generated through intersystem crossing (ISC) from singlet excitons. Furthermore, higher-lying singlet exciton states can also produce two triplet excitons through a splitting process. Therefore, the process of OLED luminescence involves the creation and recombination of excitons, resulting in light emission, with singlet excitons leading to fluorescence, which is the dominant mechanism in practical OLED devices. The luminescent mechanism can be categorized into fluorescence and phosphorescence, depending on the emitter's form. In the case of phosphorescence, singlet excitons transition to the triplet state through heavy metal elements, a process known as ISC. In the triplet state, all excitons become luminescent, significantly increasing the theoretical IQE, which allows to produce high-efficiency OLED devices.[4] On the other hand, for fluorescent materials that cannot promote the emission of triplet excitons, their internal quantum efficiency tends to be lower compared to phosphorescent materials. The thermally Activated Delayed Fluorescence (TADF) is a novel approach that theoretically allows for achieving 100% IQE by facilitating the reverse intersystem crossing (RISC), which is a triplet-singlet energy transfer between host and dopant molecules.[11] TADF molecules typically have a small ΔE_{ST} (energy gap between the lowest triplet state T_1 and singlet state S_0), enabling them to produce delayed fluorescence with extended luminescence lifetimes. TADF molecules are fluorescent, meaning that direct transitions between T_1 and S_0 states are prohibited. However, with sufficient thermal energy, RISC occurs, facilitating the transition from T_1 to S_1, followed by the emission of light when all excitons return to the ground state.[10,11] This process offers the potential for a high quantum efficiency. While using TADF molecules as the luminescent material can achieve 100% IQE, there are challenges such as lower color purity and shorter lifetime, especially for blue OLED devices. To overcome these issues, a new luminescence method called "Hyperfluorescence" has been developed by combining the advantages of both TADF and fluorescent materials.[8,10,11]

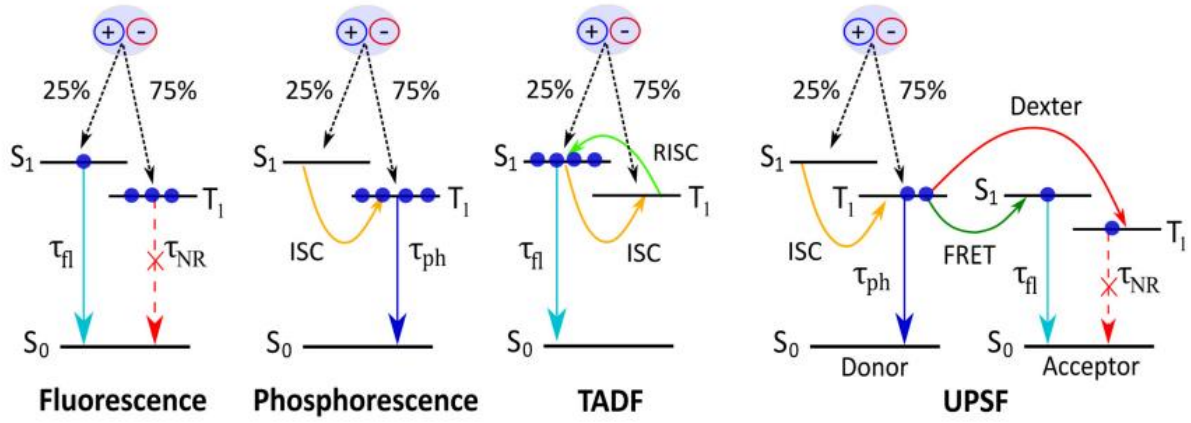

Figure 2. Various emissive paths[4]

4. Blue Fluorescence

The emission wavelength of the luminescent layer is determined by the materials used, resulting in red, green, or blue wavelengths, and the luminescent mechanism of the material distinguishes between phosphorescence and fluorescence. To enhance color purity and efficiency, the structure of the luminescent layer primarily employs a host/dopant system, where emissive species are generated in the host and emit light via transition, rather than using a single material. The emission wavelength of fluorescent luminescent materials is determined by the extent of conjugation and the polarity of the materials. In the case of blue fluorescent materials, unlike red and green, they typically require a shorter conjugation length and higher exciton energy, resulting in shorter lifetimes.[15] Consequently, the device lifetime and efficiency of blue luminescent materials have not significantly matched those of red and green luminescent materials, and research and development in this area continue.[14] To enhance the efficiency of low efficiency fluorescent luminescence, the process of triplet-triplet annihilation (TTA) is used to convert triplet excitons into singlet state, which can improve efficiency.[15] Additionally, there is a method to use phosphor-sensitized fluorescence (PSF) where triplet excitons of the phosphorescent materials are converted into singlet excitons of the fluorescent material through Förster resonance energy transfer (FRET) to emit light.[8] This allows for the development of blue luminescent materials that can achieve high efficiency and high color purity while also ensuring a long device lifetime.

5. Hyperfluorescence (HF)

The research on 3rd generation OLEDs, specifically focusing on TADF, is currently undergoing active development.[1] The core principle of TADF revolves around achieving a small energy gap, denoted as $\Delta E_{ST,}$ between singlet and triplet states, which is crucial for the RISC process. In simple terms, TADF harnesses thermal energy at room temperature to convert previously non-emissive triplet excitons into emissive singlet excitons, effectively transforming them into a fluorescent state, and achieving IQE close to 100%, just like phosphorescence.[16] However, in the pursuit of reducing $\Delta E_{ST,}$ it was necessary to lower the degree of overlap between the HOMO and LUMO. To achieve this condition, molecules needed a distinct separation of electron-donating (Donor) and electron-accepting (Acceptor) structures. This design choice resulted in significant distortion between the excited state and ground state molecular structures, which led to reduced color purity. Fortunately, these drawbacks were overcome with the introduction of Multi-resonance TADF (MR TADF). The MR effect, achieved by alternating the arrangement of HOMO and LUMO, results in short-range charge transfer (SRCT) characteristics, which in turn lead to a narrower full width at half maximum (FWHM) and higher color purity. However, another unresolved drawback is that in the case of TADF, when a large ΔE_{ST} is present, it results in slow RISC process. Consequently. Long-lived T_1 excitons accumulate, leading to issues such as external quantum efficiency (EQE) roll-off and TTA, which shorten the device lifetime. To address this reduction in device lifetime, 4th generation hyperfluorescence (HF) devices have been developed.[15] In HF devices, both host and dopant materials are co-deposited, allowing for the use of sensitizers such as phosphorescent or D-A type TADF materials. Fluorescent and MR-type TADF materials can be used as the final emitter. Energy transfer occurs from the host to the dopant.[13] When a TADF emitter is used, it undergoes an RISC process form its triplet state to the singlet state, resulting in fluorescence emission. On the other hand, if a fluorescent emitter is used, the T_1 state of the emitter is lowered to prevent Dexter Energy Transfer (DET), leading to fluorescence emission.[1,8] Therefore, by harnessing the MR effect in HF technology, it is possible to achieve high EQE and narrow-bandwidth fluorescence, enabling a broader color range in displays.

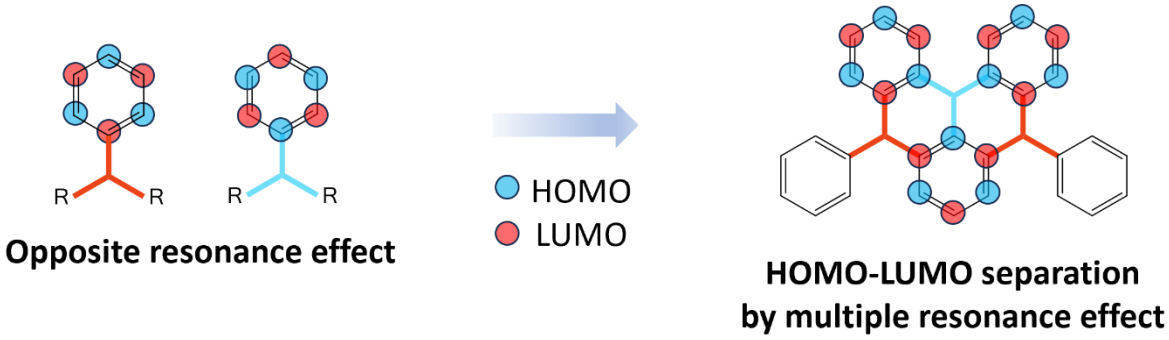

Figure 3. HOMO-LUMO separation by multiple resonance effect[12]

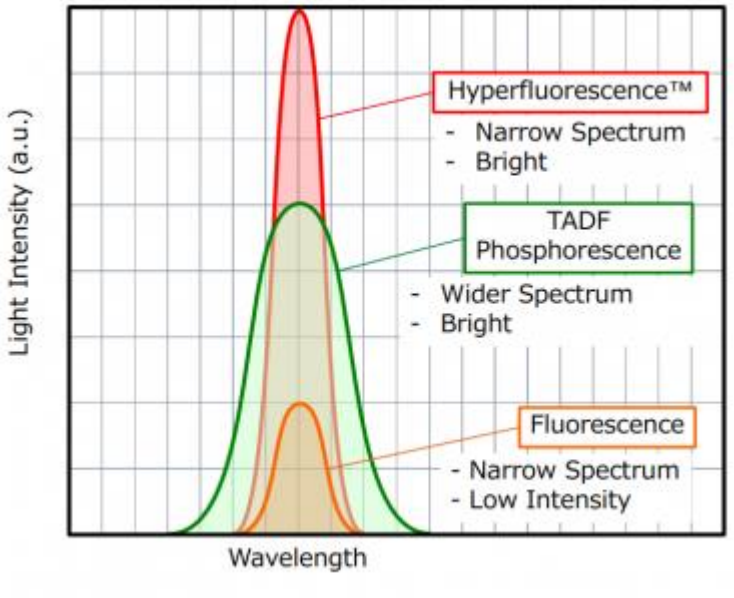

Figure 4. The narrow spectrum of hyperfluorescence[13]

6. Fluorescent emitter incorporating Polycyclic Aromatic Hydrocarbons

Polycyclic Aromatic Hydrocarbons (PAHs) are compounds that belong to the class of aromatic hydrocarbons with multiple fused rings. While most of them consist of benzene rings, azulene is an exceptional case, as it does not contain benzene rings.[18,19] The Clar's rule, named after the German chemist Erich Clar, is a principle that suggests that the more benzene rings are present in a compound, the greater its aromatic and stability, as it can accommodate more resonance structures. PAHs possess inherent fluorescent properties due to their aromatic structure, emitting light in the ultraviolet/blue spectral range. The delocalized π bonds with of the double bonds within the PAH structures make them highly fluorescent materials. This is because shared electrons within the aromatic ring are easily excited, and the strong structure does not allow effective vibrational relaxation.[19] PAH molecules originally have low triplet energies. Therefore, when introduced, the triplet energy becomes localized in the PAHs, resulting in its fluorescent properties. Exploiting this characteristic, it is possible to create compounds with various properties by incorporating PAHs into cores with different characteristics. When PAHs are introduced into cores with the MR effect, it becomes possible to design highly pure fluorescent compounds.

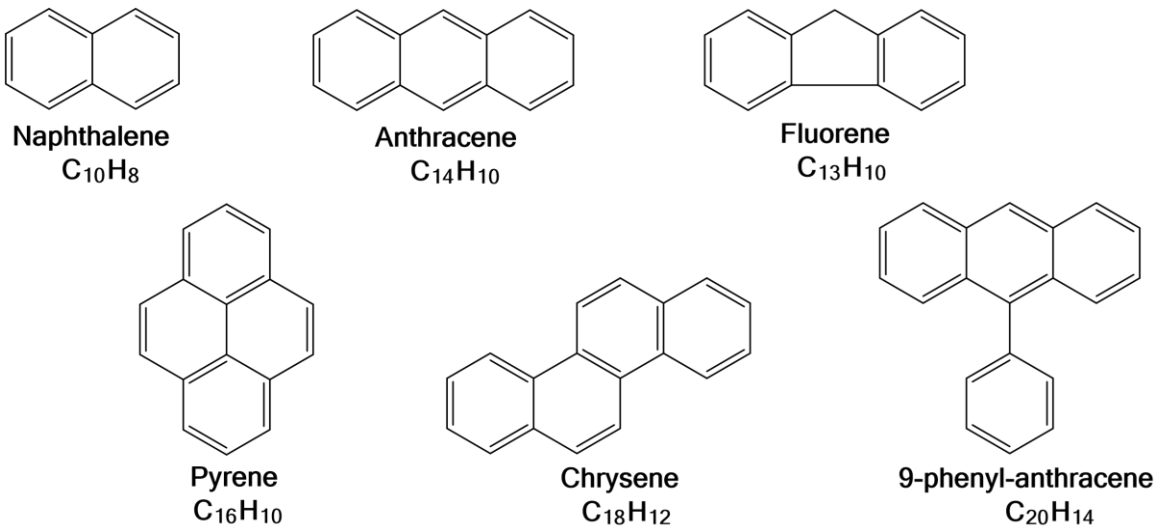

Figure 5. Representative PAHs compounds

7. Research Scopes

An OLED is a self-emissive display that utilizes organic light-emitting materials. Among the three primary colors of light, red and green have been commercialized using phosphorescent materials, but blue light sources face drawbacks due to the expensive use of rare-earth metals and short device lifetime. As a result, blue light sources predominantly rely on fluorescent materials, which exhibit issues related to low device efficiency. To address these challenges, recent developments in the field have introduced HF OLEDs utilizing DABNA-based MR TADF emitters, known for their high efficiency and color purity. However, MR-TADF emitters suffer from a prolonged triplet state lifetime, leading to severe chemical decomposition processes in the triplet state. To improve device lifetime and color purity, it is essential to develop emitters that do not undergo delayed fluorescence. In this study, we attempted to develop a high stability blue fluorescence emitter for HF OLEDs by incorporating PAHs, multi-ring aromatic hydrocarbons with low triplet energy, into a DABNA scaffold with a diboron atom system. By introducing PAH moieties to the DABNA emitter core, we induced a lower triplet state (T_1) energy, thus preventing DET and promoting non-radiative decay of the triplet state. This was aimed at ultimately enhancing the device lifetime and achieving a high-color purity blue fluorescence. To accomplish this, we synthesized compounds, namely **Xyl-diOBN-Pyr** and **Xyl-diOBN-Ph-ant**, by introducing PAH moieties at the para position of the diboron DABNA core. We analyzed their molecular structures using NMR spectroscopy and elemental analysis. Through analyses of their optical absorption, emission spectra and photoluminescence properties, we observed the blue fluorescence properties. Based on this, we conducted research to investigate the changes in the triplet state and photophysical properties of the DABNA structure resulting from the introduction of PAH moieties.

II. Experiment

1. Chemical and instrumentation

All operations were performed under an inert nitrogen atmosphere using standard Schlenk and glovebox techniques. Anhydrous grade solvents (Aldrich) were dried by passing them through an activated alumina column and stored over activated molecular sieves (5 Å). Spectrophotometric-grade solvents for photophysical measurements were used as received from Aldrich and Merck. Commercial reagents were used without further purification after purchase. Deuterated solvents from Cambridge isotope Laboratories were used. NMR spectra were recorded on a Bruker Avance III HD (400 MHz for ^{1}H, 100 MHz for ^{13}C) spectrometer at ambient temperature. Chemical shifts are given in parts per million (ppm), and are referenced against external Me_4Si (^{1}H, ^{13}C). Elemental analyses were performed on a Flash 2000 elemental analyzer (Thermo Scientific) at University of Ulsan. Melting points (mp) were measured by Melting Point Apparatus SMP30 (Stuart Equipment). Thermogravimetric analysis (TGA) was performed with a TA Instruments Q50 under an N_2 atmosphere at a heating rate of 10 °C/min. Mass spectra were obtained on a JEOL JMS700 high-resolution FAB-mass spectrometer (HR FAB-MS) at the Korea Basic Science Institute, Daegu, Korea. Cyclic voltammetry experiments were performed using an Autolab/PGSTAT101 system.

2. Synthesis

All compounds were prepared according to **Scheme 1.** 1-bromo-3-chloro-5-(m-tolyloxy)benzene and *N*1,*N*3-bis(3,5-dimethylphenyl)benzene-1,3-diamine were prepared from the reported procedure.[20, 21] Full experimental details are given below.

_N_1,_N_3-bis(3-chloro-5-(m-tolyloxy)phenyl)-_N_1,_N_3-bis(3,5-dimethylphenyl)benzene-1,3-diamine (1, Final liand of Xyl-diOBN-Cl)

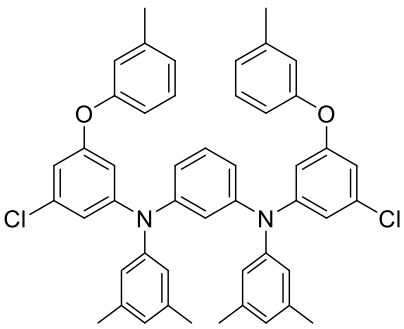

The mixture of 1-bromo-3-chloro-5-(m-tolyloxy)benzene (1 g, 3.16 mmol), *N*1,*N*3-bis(3,5-dimethylphenyl)benzene-1,3-diamine (2.07 g, 6.95 mmol), tris-(dibenzylideneacetone)dipalladium(0) ($Pd_2(dba)_3$, 0.08 g, 0.09 mmol), tri-*tert* butyl phosphonium tetrafluoroborate (0.06 g, 0.19 mmol), and sodium *tert*-butoxide (0.91 g, 9.48

mmol) was dissolved in dry toluene (35 mL), then the mixture was heated at 90 °C for 24 h. After cooling down, the mixture was diluted with CH_2Cl_2, filtered through celite pad, and concentrated under reduced pressure. The crude product was subjected to silica gel column chromatography using CH_2Cl_2/hexane (1:4, v/v). The corresponding fractions were combined and the solvents were removed under reduced pressure,the product was obtained as white solid (yield: 1.5 g, 63%). ^{1}H NMR (400 MHz, CD_2Cl_2) δ 7.20 (t, J = 5.6 Hz, 2H), 7.16 (d, J = 8.1 Hz, 1H), 6.93 (d, J = 7.5 Hz, 2H), 6.83 (t, J = 1.9 Hz, 1H), 6.79 (s, 2H), 6.75 (dd, J = 7.7, 5.6 Hz, 4H), 6.72 (s, 2H), 6.70 (s, 4H), 6.64 (t, J = 1.8 Hz, 2H), 6.53 (t, J = 2.0 Hz, 2H), 6.44 (t, J = 1.9 Hz, 2H), 2.31 (s, 6H), 2.21 (s, 12H); ^{13}C NMR (101 MHz, CD_2Cl_2) δ 159.10, 156.61, 150.45, 148.34, 146.67, 140.58, 139.65, 135.39, 130.50, 129.84, 126.49, 125.02, 123.57, 121.73, 120.53, 120.20, 116.92, 116.46, 111.75, 111.05, 21.41; HRMS (EI) *m/z* calcd for $C_{48}H_{42}Cl_2N_2O_2$ 748.26, observed 748.2619.

Xyl-diOBN-Cl (2)

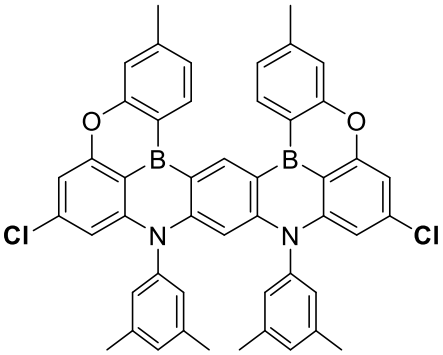

Boron triiodide (1.14 g, 2.93 mmol) and **1** (1 g, 1.33 mmol) were dissolved 1,2,4-trichlorobenzene (35 mL) under a nitrogen atmosphere. After stirring at 60 °C for 24 h, the reaction mixture was allowed to cool to room temperature. After phosphate-buffered saline (*p*H 7.4, 100 mL), and dried over magnesium sulfate. After the solvent was removed *in vacuo*, the residue was filtered with silica gel column chromatography (eluent: CH_2Cl_2). The product was obtained as a yellow solid (yield: 0.55 g, 54%). ^{1}H NMR (400 MHz, CD_2Cl_2) δ 10.38 (s, 1H), 8.92 (d, J = 8.2 Hz, 2H), 7.40 (d, J = 4.0 Hz, 4H), 7.13 (s, 2H), 7.05 (d, J = 1.6 Hz, 2H), 6.71 (s, 4H), 6.33 (d, J = 1.5 Hz, 2H), 5.85 (s, 1H), 2.58 (s, 6H), 2.34 (s, 12H); ^{13}C NMR (101 MHz, $C_2D_2Cl_4$) δ 159.35, 157.79, 149.93, 146.33, 143.84, 143.30, 140.16, 139.76, 138.17, 133.57, 129.48, 126.05, 124.20, 119.76, 117.95, 117.64, 113.09, 107.78, 106.22, 103.90, 21.38, 20.81; HRMS (EI) *m/z* calcd for $C_{48}H_{36}B_2Cl_2N_2O_2$ 764.23, observed 764.2341.

Xyl-diOBN-Pyr (3)

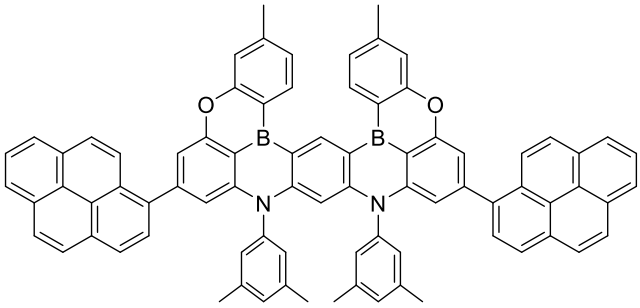

Pyren-1-ylboronic acid (0.2 g, 0.82 mmol), **2** (0.25 g, 0.33 mmol), tris-(dibenzylideneacetone)dipalladium(0) ($Pd_2(dba)_3$, 0.02g, 0.02 mmol), Xphos (0.02g, 0.05 mmol), and potassium phosphate tribasic (0.21 g, 0.99 mmol) were dissolved in toluene/H_2O (10:1, 33 mL) under a nitrogen atmosphere. After stirring at 110 °C for 3 days, the crude product was subjected to silica gel column chromatography using CH_2Cl_2/hexane (1:5, v/v). The corresponding fractions were combined and the solvents were removed under reduced pressure,the product was obtained as a yellow solid (yield: 0.32 g, 90%). ^{1}H NMR (400 MHz, CD2Cl2) δ 10.56 (s, 1H), 9.08 (d, J = 8.1 Hz, 2H), 8.25 (s, 1H), 8.22 (d, J = 7.8 Hz, 5H), 8.19 (s, 1H), 8.17 (s, 1H), 8.11 (s, 4H), 8.05 (s, 1H), 8.03 (s, 1H), 8.02 (s, 2H), 8.00 (s, 2H), 7.47 (s, 4H), 7.36 (s, 2H), 6.93 (s, 2H), 6.84 (s, 4H), 6.65 (s, 2H), 6.02 (s, 1H), 2.64 (s, 6H), 2.24 (s, 12H); ^{13}C NMR (101 MHz, $C_2D_2Cl_4$) δ 161.42, 158.99, 151.89, 147.10, 145.61, 144.73, 141.92, 141.46, 138.80, 135.43, 132.41, 131.88, 131.67, 130.79, 129.39, 128.83, 128.78 – 128.26, 127.77, 127.33, 126.43, 126.14, 125.68, 121.87, 119.66, 119.08, 115.43, 112.03, 109.51, 105.33, 32.18, 23.08, 22.34; Anal. Calcd for $C_{80}H_{54}B_2N_2O_2$: C, 87.60; H, 4.96; N, 2.55. Found: C, 86.86; H, 4.80; N, 2.50; T_{d5} = 461 °C.

Xyl-diOBN-Ph-ant (4)

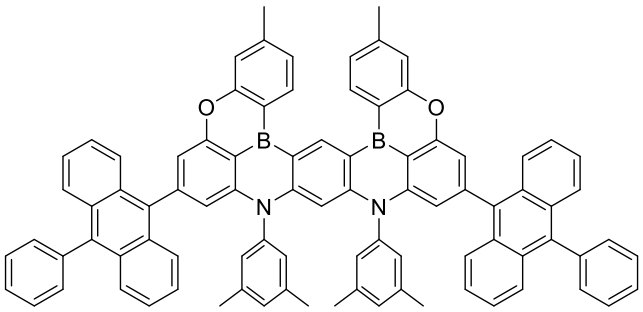

(10-phenylanthracen-9-yl)boronic acid (0.25 g, 0.85 mmol), **2** (0.25 g, 0.33 mmol), tris-(dibenzylideneacetone)dipalladium(0) ($Pd_2(dba)_3$, 0.02g, 0.02 mmol), Xphos (0.02g, 0.05 mmol), and potassium phosphate tribasic (0.21 g, 0.99 mmol) were dissolved in toluene/H_2O (10:1, 33 mL) under a nitrogen atmosphere. After stirring at 110 °C for 3 days, the crude product was subjected to silica gel column chromatography using CH_2Cl_2/hexane (1:5, v/v). The corresponding fractions were combined and the solvents were removed under reduced pressure,the product was obtained as a yellow solid (yield: 0.32 g, 82%). ^{1}H NMR (400 MHz, CD2Cl2) δ 10.64 (s, 1H), 9.14 (d, J = 7.8 Hz, 2H), 7.84 – 7.80 (m, 4H), 7.67 (dd, J = 7.3, 2.9 Hz, 6H), 7.64 (s, 2H), 7.62 (s, 2H), 7.60 (s, 1H), 7.52 (dd, J = 10.6, 4.5 Hz, 6H), 7.43 (d, J = 7.7 Hz, 2H), 7.38 – 7.32 (m, 8H), 7.25 (d, J = 0.9 Hz, 2H), 6.91 (s, 2H), 6.82 (s, 3H), 6.56 (d, J = 0.9 Hz, 2H), 6.03 (s, 1H), 2.67 (s, 6H), 2.20 (s, 12H); ^{13}C NMR (101 MHz, $C_2D_2Cl_4$) δ 161.35, 160.98 – 160.21, 155.46, 148.88 – 148.24, 148.88 – 147.42, 147.35, 146.53, 146.53, 148.88 – 144.94, 145.80, 147.42 – 140.41, 139.08, 140.41 – 135.56, 140.41 – 132.21, 130.71, 130.47, 129.69 – 127.85, 128.19 – 127.25, 128.55 – 127.85, 126.23, 125.68, 121.85, 119.66, 119.12, 115.74, 112.61, 110.77, 105.44, 23.07, 22.34; Anal. Calcd for $C_{88}H_{62}B_2N_2O_2$: C, 88.00; H, 5.20; N, 2.33. Found: C, 87.67; H, 5.00; N, 2.33; T_{d5} = 490 °C.

3. Photophysical measurements

UV/Vis absorption and photoluminescence (PL) spectra were measured on a Varian Cary 100 and an FLS1000 (Edinburgh Instrument) spectrophotometer at 298 K, respectively. The solution PL spectra were obtained from a nitrogen bulbbled solution prepared in a glovebox at ambient conditions. (typically 10 μM in toluene). The photoluminescence quantum yields (PLQYs, Φ_{PL}) of solutions were measured on an absolute PL quantum yield spectrophotometer (Quantaurus-QY C11347-11, Hamamatsu Photonics) equipped with a 3.3-inch integrating sphere. Transient PL decays were recorded on an FLS1000 spectrophotometer (Edinburgh Instruments) in either time-correlated single-photon counting (TCSPC) mode (EPL-375 picosecond pulsed diode laser as a light source) for the prompt fluorescence region and a milti-channel scaling (MCS) mode (VPL-375 diode laser) for the delayed fluorescence region. The photophysical analysis done by using FLS1000 and Quantaurus-QY spectrophotometers were carreid out at Total-Period Analysis Center for Ulsan Chemical Industry of KBSI.

4. Cyclic voltammetry

Cyclic voltammetry measurements were carried out in CH_2Cl_2 (1.0×10^{-3} M) with a three-electrode cell configuration consisting of platinum working and counter electrodes and an $Ag/AgNO_3$ (0.01 M in CH_3CN) reference electrode at room temperature. Tetra-*n*-butylammonium hexafluorophosphate (0.1 M) was used as the supporting electrolyte. The oxidation potentials were recorded at a scan rate of 100 mV/s and are reported against the ferrocene/ferrocenium (Fc/Fc^+) redox couple. The HOMO energy levels were determined from the electrochemical oxidation cyclic voltammograms while the LUMO energy levels were estimated from the optical bandgap (E_g) and the HOMO levels.

III. Results and Discussion

1. Synthesis and characterization

Xyl-diOBN-PAH compounds, namely **Xyl-diOBN-Pyr** and **Xyl-diOBN-Ph-ant** were prepared according to **Scheme 1**. Commercially available 1-bromo-3-chloro-5-fluorobenzene and diiodobenzene coupled successively with m-cresol and 3,5-dimethylaniline respectively to give the desired dichloro-intermediate **1**. Noteworthily, it was carried out through a one-shot borylation using BI3, producing Xyl-diOBN-Cl in a reasonable yield (54%). Finally, PAH groups were introduced at the outer chloro site through coupling with pyren-1-ylboronic acid and (10-phenylanthracen-9-yl)boronic acid to form **Xyl-diOBN-Pyr** and **Xyl-diOBN-Ph-ant**, respectively. The **Xyl-diOBN-Pyr** and **Xyl-diOBN-Ph-ant** were characterized by multinuclear NMR spectroscopy (**Figure 6–9**) and elemental analysis (EA).

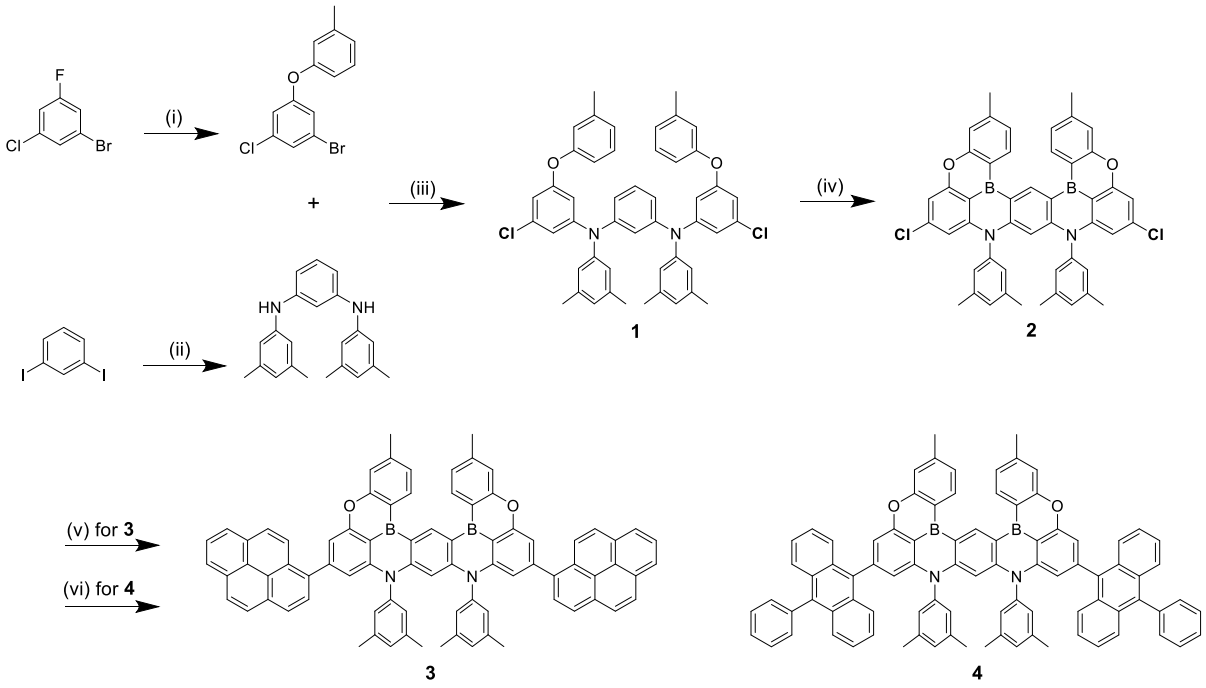

Scheme 1. Synthesis of **1–4**. Conditions and reagents Condition: (i) m-cresol, K_2CO_3, N-Methyl-2-Pyrrolidone, 150 °C, o/n; (ii) 3,5-Dimethylaniline, $Pd_2(dba)_3$, DPEphos, NaO^{t}Bu, toluene, 80 °C, o/n; (iii) $Pd_2(dba)_3$, tBu$_3$PHBF$_4$, NaO^{t}Bu, toluene, 90 °C, o/n; (iv) Boron triiodide, 1,2,4-Trichlorobenzene, 60 °C, o/n; (v) pyren-1-ylboronic acid, $Pd_2(dba)_3$, Xphos, K_3PO_4, toluene/H_2O (10:1), reflux, 3 d; (vi) (10-phenylanthracen-9-yl)boronic acid, $Pd_2(dba)_3$, Xphos, K_3PO_4, toluene/H_2O (10:1), reflux, 3 d.

The ^{1}H NMR spectra of **Xyl-diOBN-Pyr** and **Xyl-diOBN-Ph-ant** exhibits sharp singlet (δ 10.56 ppm and δ 10.64 ppm) and doublet (δ 9.07, 9.09 ppm and δ 9.13, 9.15 ppm) of near boron. Furthermore, from TGA analysis shows thermal stability, giving T_{d5} value of 461 ºC, 490 ºC for **Xyl-diOBN-Pyr** and **Xyl-diOBN-Ph-ant** respectively.

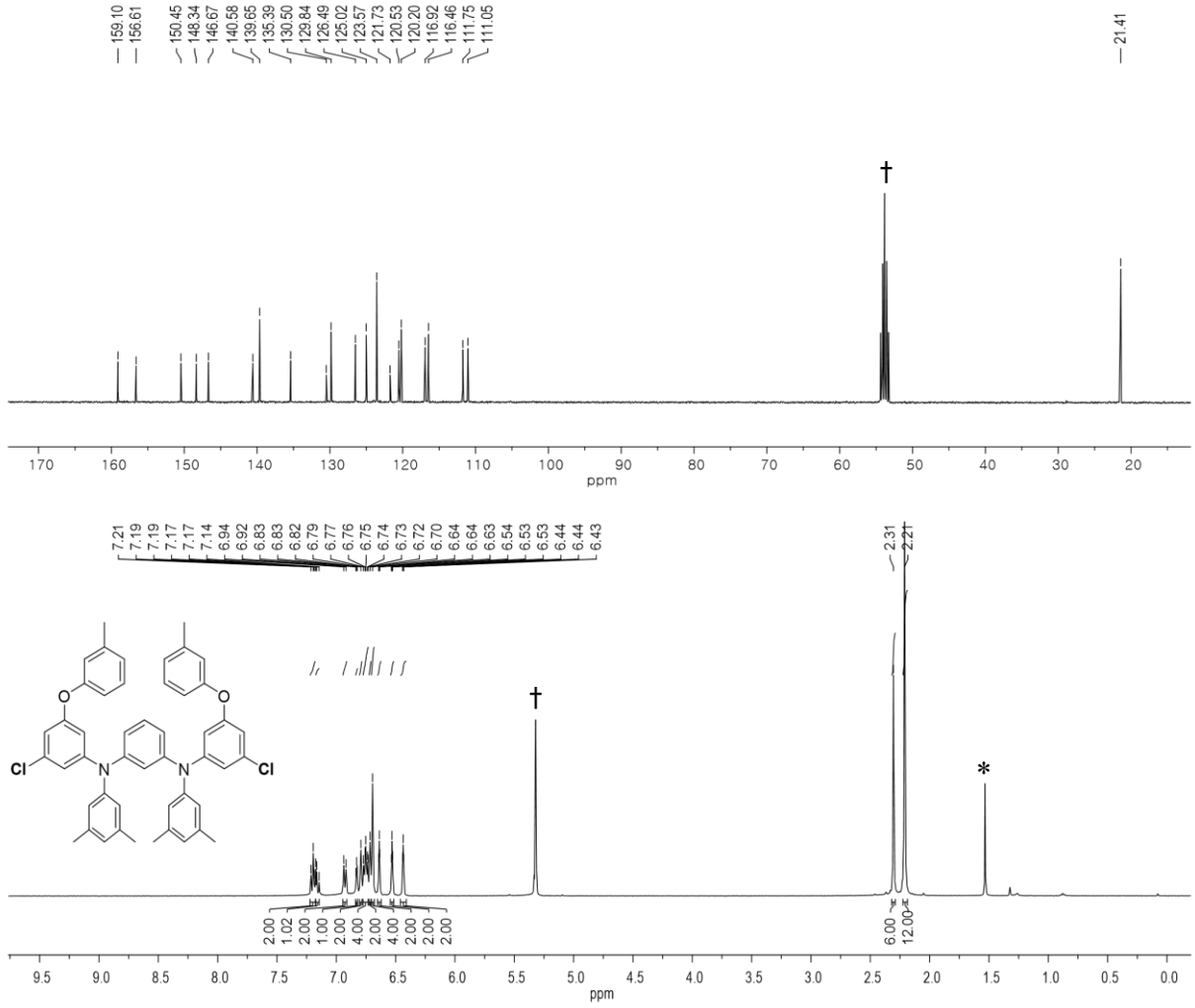

Figure 6. ^{1}H (bottom) and ^{13}C (top) NMR spectra of **1** in CD_2Cl_2 (* from residual H_2O, † from CH_2Cl_2).

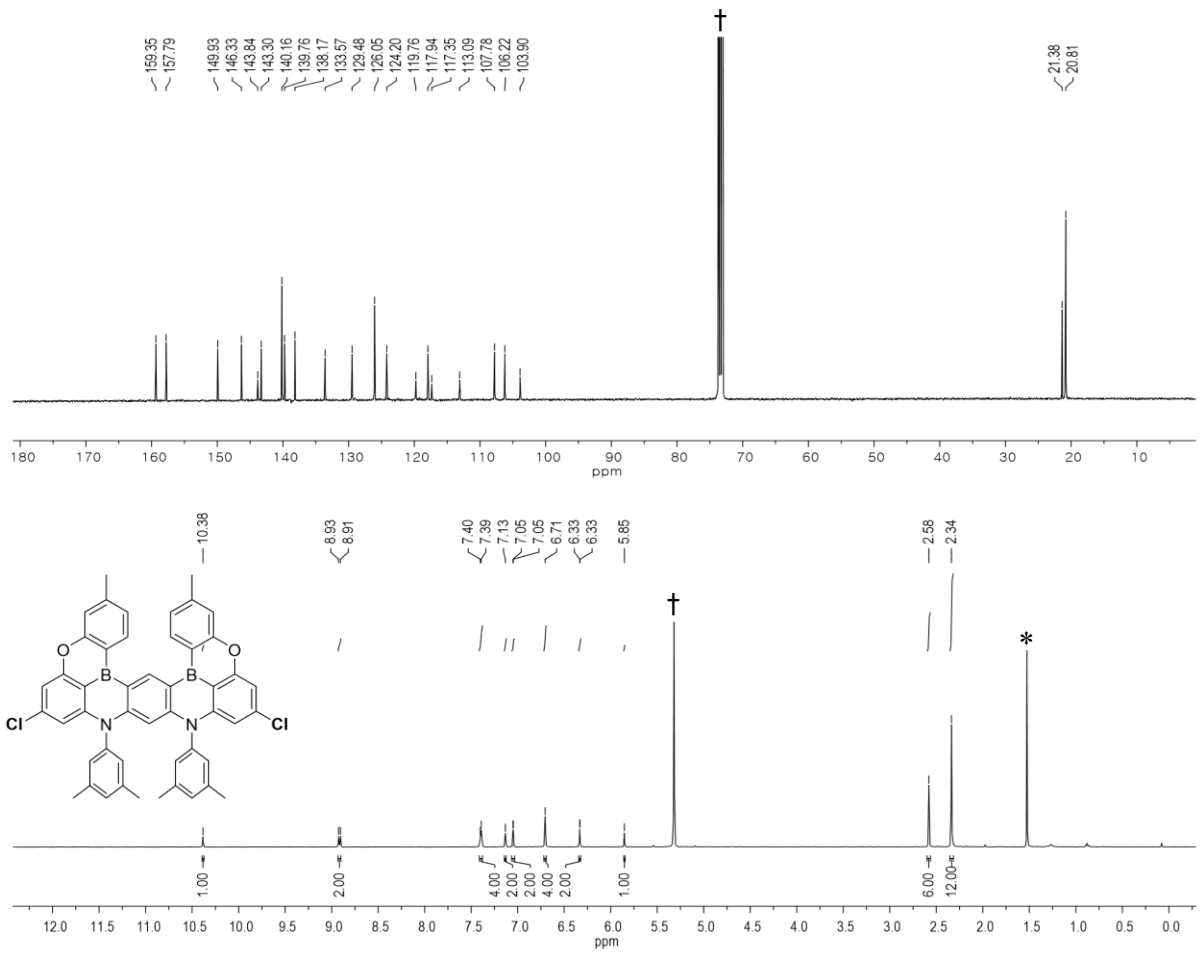

Figure 7. ^{1}H (bottom) NMR spectra of **2** in CD_2Cl_2 (* from residual H_2O, † from CH_2Cl_2).

^{13}C (top) NMR spectra of **2** in $C_2D_2Cl_4$ (* from residual H_2O, † from $C_2H_2Cl_4$).

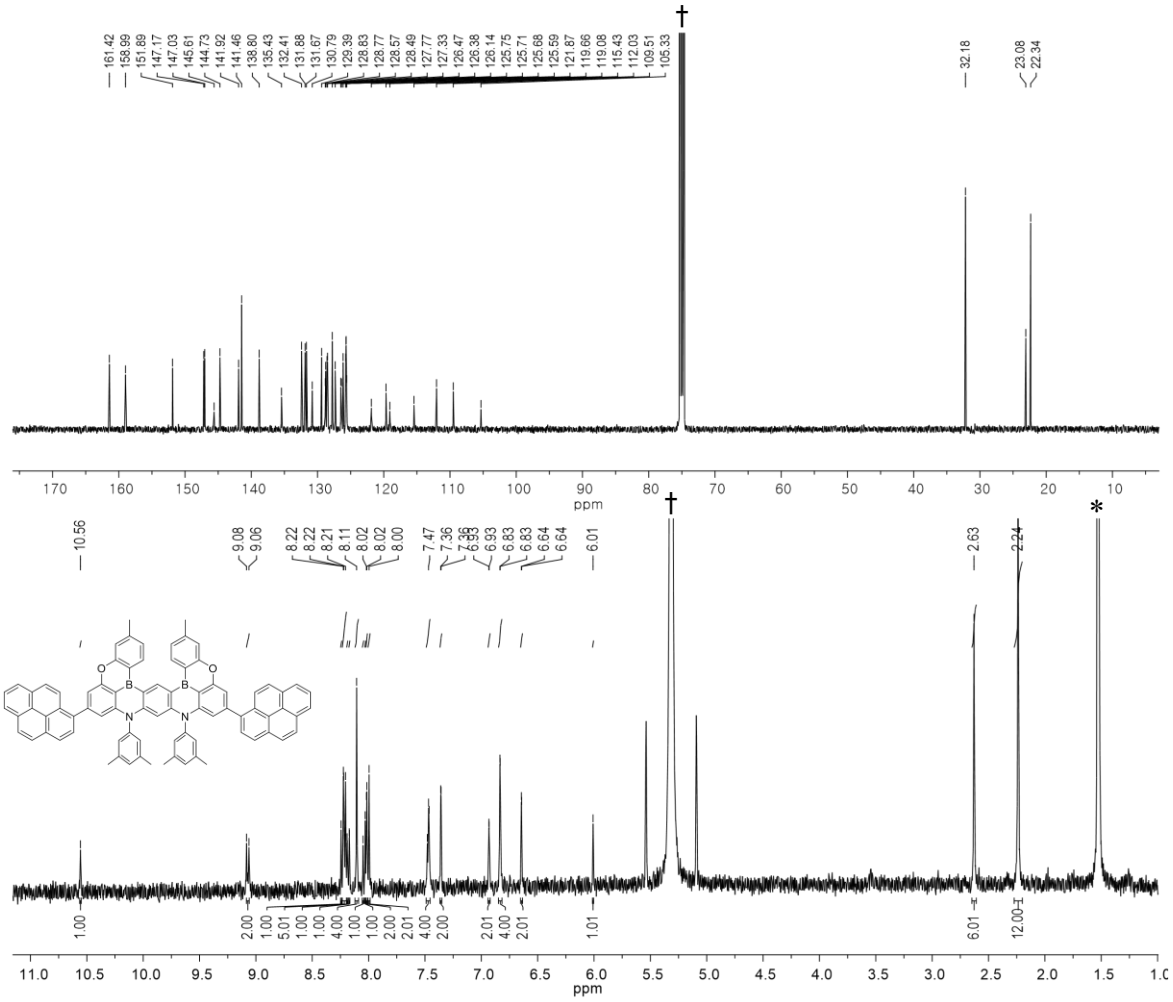

Figure 8. ^{1}H (bottom) NMR spectra of **3** in CD_2Cl_2 (* from residual H_2O, † from CH_2Cl_2).

^{13}C (top) NMR spectra of **3** in $C_2D_2Cl_4$ (* from residual H_2O, † from $C_2H_2Cl_4$).

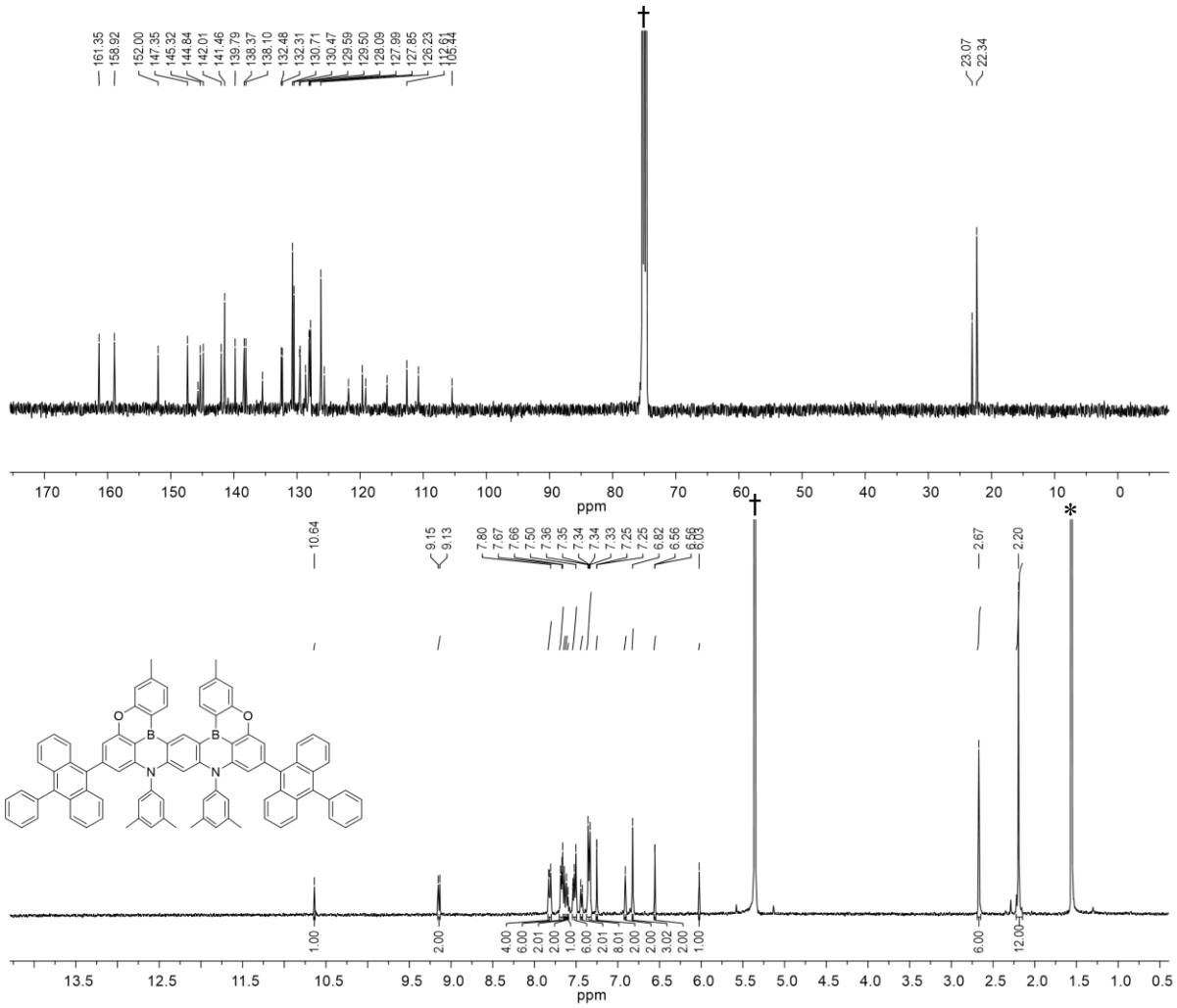

Figure 9. ^{1}H (bottom) NMR spectra of **4** in CD_2Cl_2 (* from residual H_2O, † from CH_2Cl_2).

^{13}C (top) NMR spectra of **4** in $C_2D_2Cl_4$ (* from residual H_2O, † from $C_2H_2Cl_4$).

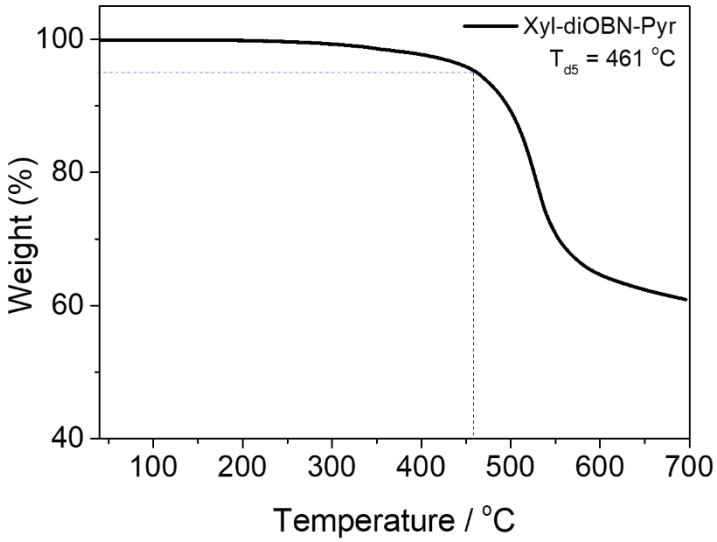

Figure 10. TGA curve of **Xyl-diOBN-Pyr**

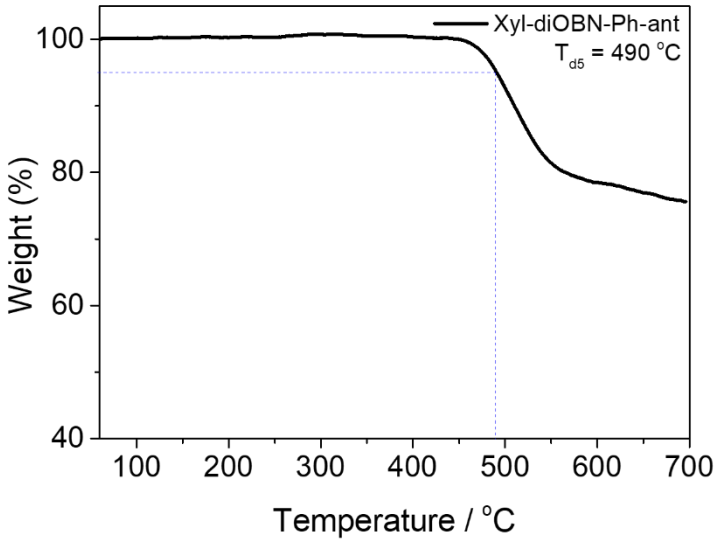

Figure 11. TGA curve of **Xyl-diOBN-Ph-ant**

2. Photophysical Properties

The photophysical properties of all compounds, including UV/Vis absorption and photoluminescence (PL) spectra, were measured in degassed toluene (1.0×10^{-5} M) (**Figure 12** and **Table 1**). All compounds showed ππ* transition bands below 400 nm whereas intense short-range charge transfer (SRCT) was similarly observed at 400-480 nm in dilute toluene solution. The PL spectra which is deep blue color emission (**Xyl-diOBN-Pyr** = 455 nm; **Xyl-diOBN-Ph-ant** = 450 nm). The PL spectra peaks of the two compounds containg PAH exhibited narrow and identical FWHM values of 21 nm. Meanwhile, PLQYs (74-99%) and short fluorescence lifetimes (4.87−5.13 ns) were retained in **Xyl-diOBN-Pyr** and **Xyl-diOBN-Ph-ant**, indicating typical MR character with fast radiative decay of the S_1 excited states. Next, the S_1 and T_1 states of the compounds were estimated from the emission peaks of fluorescence (FL) and phosphorescence (PH) spectra in a frozen toluene matrix at 77 K (**Figure 14** and **Table 2**). The T_1 energies of **Xyl-diOBN-Pyr** and **Xyl-diOBN-Ph-ant** were calculated to be 2.02 eV and 1.76 eV, respectively. In fact, the observed low T_1 energy corresponds to the triplet excited state of pristine pyrene and phenylanthracene. Significantly larger ΔE_{ST} values of 0.70 eV for **Xyl-diOBN-Pyr** and 0.99 eV for **Xyl-diOBN-Ph-ant** were estimated. Thus, it is anticipated that the RISC process would hardly take pace in **Xyl-diOBN-Pyr** and **Xyl-diOBN-Ph-ant**. To confirm the fluorescence of the compounds, we next investigated the photophysical properties of 2 wt% doped films in a PMMA matrix (**Figure 15** and **Table 3**). The PL emission shows a slight red-shifted and a somewhat broadened FHWM when compared to the data of the solution.

Table 1. Photophysical data of **Xyl-diOBN-Pyr** and **Xyl-diOBN-Ph-ant**

Compound	λ_{abs}[a] [nm]	λ_{PL}[a] [nm]	Φ_{PL}[b] (%) In N_2	FWHM[c] [nm]	τ_p[d][ns]
Xyl-diOBN-Pyr	357, 440	455	0.99	21	4.87
Xyl-diOBN-Ph-ant	337, 357, 377, 397, 436	450	0.74	21	0.99

[a] toluene at 298 K (10×10^{-6} M); [b] Absolute photoluminescence quantum yields (PLQYs) in oxygen-free (N_2) toluene at 298 K; [c] Full Width at Half Maxima; [d] Prompt (τ_p) PL lifetimes in oxygen-free toluene solutions at 298 K.

Table 2. Photophysical data of **Xyl-diOBN-Pyr** and **Xyl-diOBN-Ph-ant** at 77 K

Compound	λ_{PL}[a] [nm]	E_S[b] [eV]	E_T[b] [eV]	ΔE_{ST}[c] [eV]
Xyl-diOBN-Pyr	456	2.72	2.02	0.70
Xyl-diOBN-Ph-ant	450	2.75	1.76	0.99

[a] toluene at 77 K (10×10^{-6} M); [b] E_S and E_T were calculated from the peak wavelength of fluorescence and phosphorescence spectra respectively at 77 K; [c] $\Delta E_{ST} = E_S - E_T$.

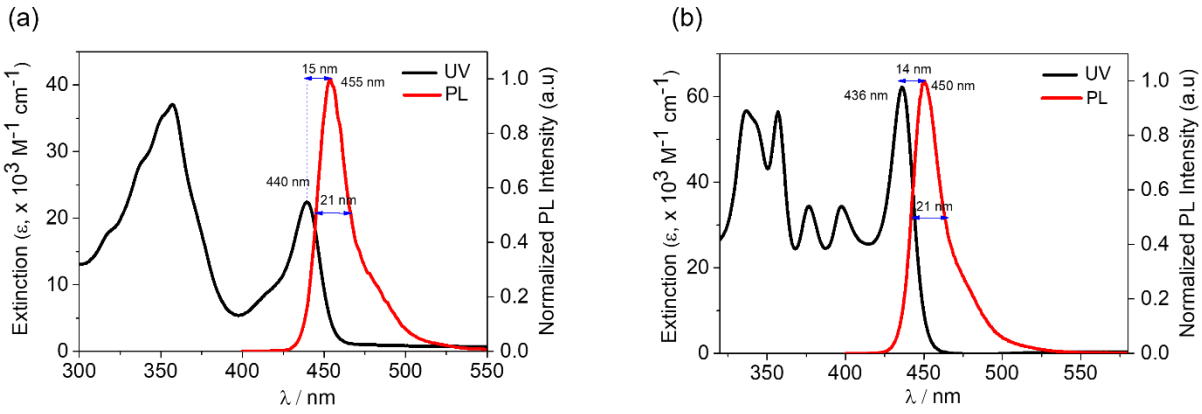

Figure 12. UV/vis absorption and PL spectra of (a) **Xyl-diOBN-Pyr**, (b) **Xyl-diOBN-Ph-ant** in toluene (1.0×10^{-5} M) at 298 K. The absorption and emission maximum wavelengths, Stokes shifts, and FWHMs are provided.

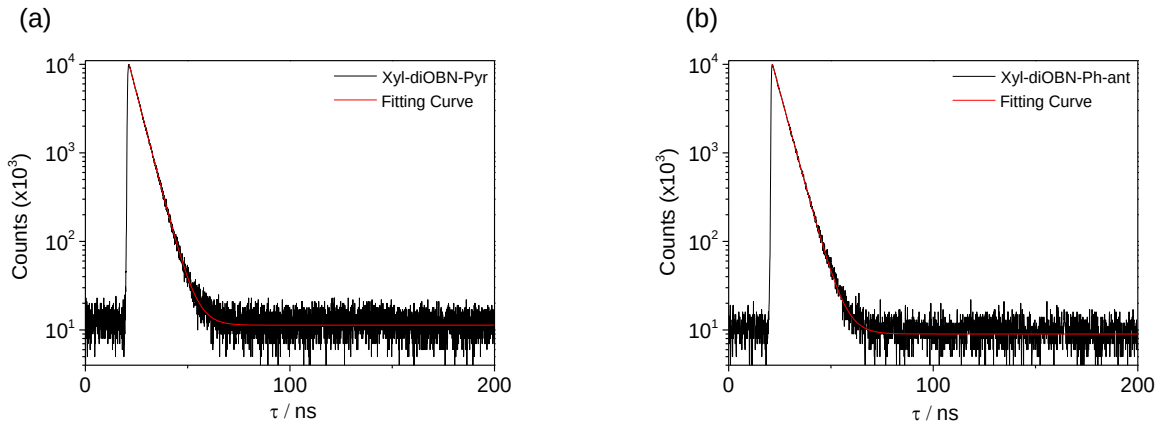

Figure 13. Transient PL decay curves of (a) **Xyl-diOBN-Pyr,** (b) **Xyl-diOBN-Ph-ant** in toluene at 298 K.

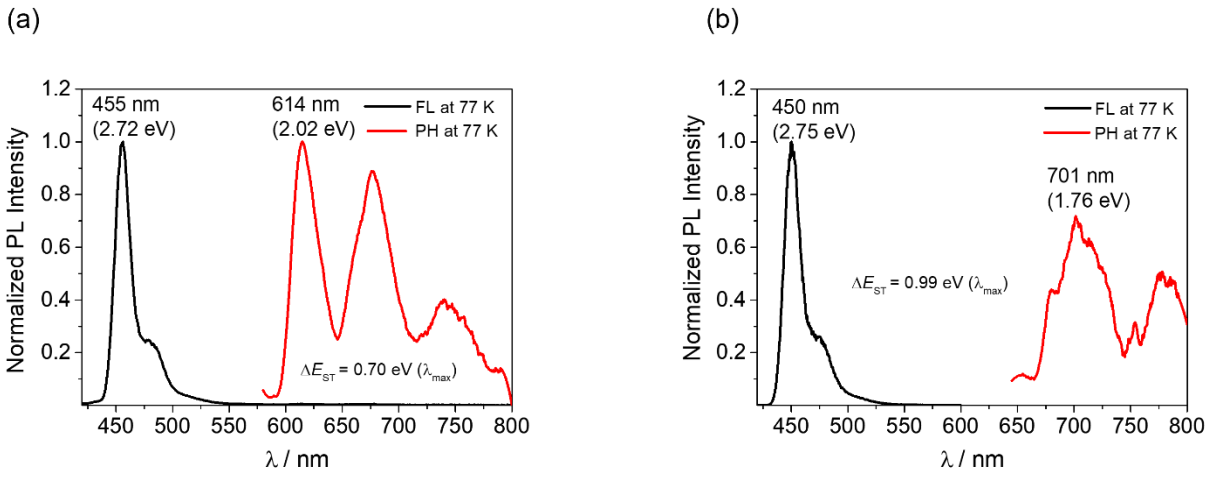

Figure 14. Fluorescence (FL) and phosphorescence (PH) spectra of (a) **Xyl-diOBN-Pyr**, (b) **Xyl-diOBN-Ph-ant** in toluene (1.0×10^{-5} M).

Table 3. Photophysical data of **Xyl-diOBN-Pyr** and **Xyl-diOBN-Ph-ant** in PMMA film

Compound	λ_{PL}[a] [nm]	Φ_{PL}[b] (%) In N_2	FWHM[c] [nm]	τ_p[d] [ns]
Xyl-diOBN-Pyr	464	0.72	34	5.14
Xyl-diOBN-Ph-ant	463	0.69	58	2.77

[a)] PMMA films doped with 2 wt% at 298 K; [b)] Absolute photoluminescence quantum yields (PLQYs) in PMMA films doped with 2 wt% at 298 K; [c)] Full Width at Half Maxima; [d)] Prompt (τ_p) PL lifetimes in PMMA films doped with 2 wt% at 298 K.

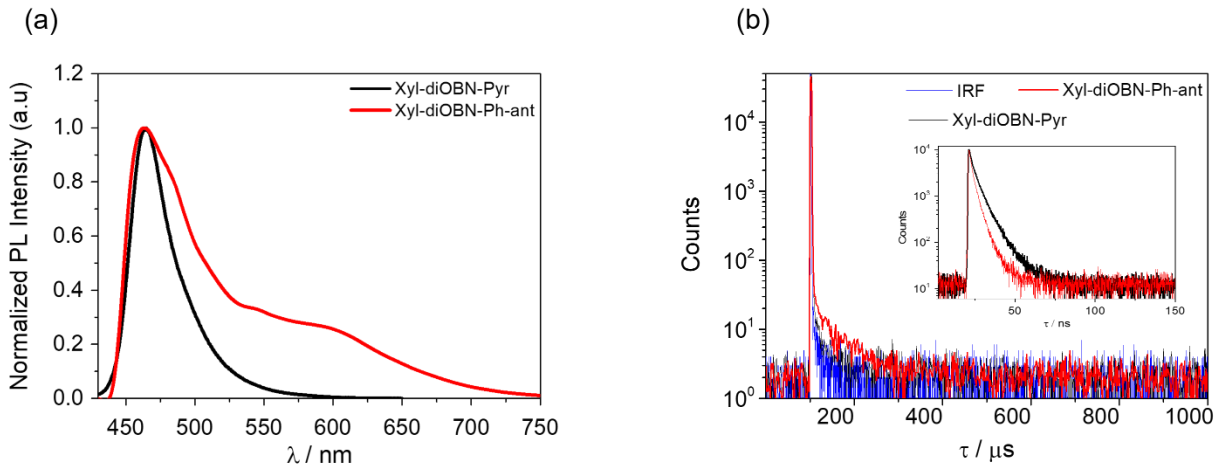

Figure 15. Photophysical properties of 2 wt% doped films in a PMMA matrix.

3. Electrochemical Properties

The electrochemistry properties of **Xyl-diOBN-Pyr** and **Xyl-diOBN-Ph-ant** were carried out by cyclic voltammetry **(Figure 14** and **Table 3**). The HOMO energy levels were determined from the electrochemical oxidation cyclic voltammograms while the LUMO energy levels were estimated from the optical bandgap (E_g) and the HOMO levels. Thus, the oxidation potentials were 0.726 eV (**Xyl-diOBN-Pyr**) and 0.781 eV (**Xyl-diOBN-Ph-ant**). Consequently, their HOMO energy levels were –5.53 eV (**Xyl-diOBN-Pyr**) and –5.58 eV (**Xyl-diOBN-Ph-ant**). All reduction potentials were estimated from the optical band gap (E_g) and the HOMO levels, giving their calculated LUMO energy levels were –2.82 eV and –2.84 respectively.

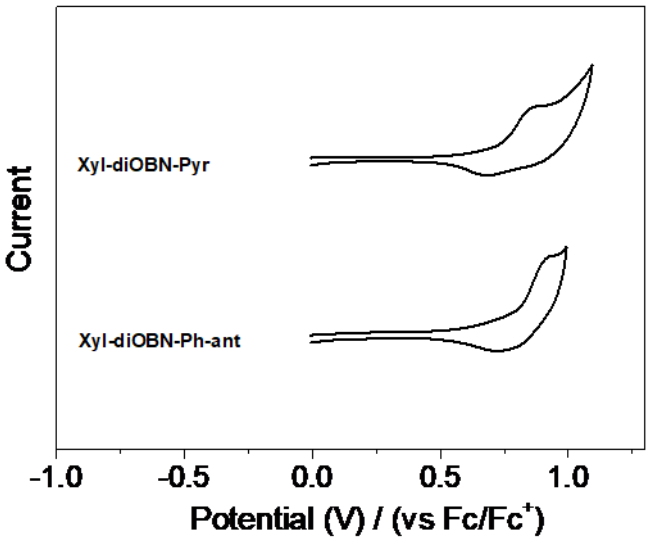

Figure 16. Cyclic voltammograms of **Xyl-diOBN-Pyr** and **Xyl-diOBN-Ph-ant** (1.0×10^{-3} M in DCM, scan rate = 100 mV/s).

Table 4. Electrochemical data of **Xyl-diOBN-Pyr** and **Xyl-diOBN-Ph-ant**

Compound	E_{ox}[a] [eV]	HOMO/LUMO[b] [eV]	E_g[c] [eV]
Xyl-diOBN-Pyr	0.726	–5.53/–2.82	2.71
Xyl-diOBN-Ph-ant	0.781	–5.58/–2.84	2.74

[a] Oxidation in DCM at 298 K (1.0×10^{-3} M in 0.1 M $TBAPF_6$ as electrolyte); [b] HOMO (eV) = $-(E_{ox} + 4.8)$; [c] E_g = optical bandgap from the absorption onset wavelength.

IV. Conclusion

DABNA-type **Xyl-diOBN-Pyr** and **Xyl-diOBN-Ph-ant** compounds were prepared and characterized through NMR spectroscopy, elemental analysis. All compounds in solution exhibit fluorescence which was characterized by UV/Vis, PL, PLQY and lifetime measurements. All compounds show the normal PLQY in in the oxygen free toluene (Φ_{PL} = 74–99%). And they have good thermal stability (T_{d5} = 461 °C for **Xyl-diOBN-Pyr**; 490 °C for **Xyl-diOBN-Ph-ant**) due to its rigidly fixed structure by π-conjugation. The presence of the low T_1 units effectively lowered the T_1 energy of the emitter, leading to a substantial increase in ΔE_{ST} and resulting in a narrow FWHM and high PLQY due to the MR-core. These photophysical properties suggest that the T_1 excited state is localized on the low T_1 units, thereby suppressing the accumulation of long-lived T_1 excitons in the emitter. We anticipate that this research holds promise for achieving highly efficient and stable blue OLEDs.

V. Reference

1. Hong, G., Gan, X., Leonhardt, C., Zhang, Z., Seibert, J., Busch, J. M., Bräse, S., A Brief History of OLEDs—Emitter Development and Industry Milestones. *Adv. Mater*. **2021**, 33, 2005630.
2. Liu, Y.-F.; Feng, J.; Bi, Y.-G.; Yin, D.; Sun, H.-B. Recent Developments in Flexible Organic Light-Emitting Devices. *Adv. Mater. Technol*. **2019**, 4, 1800371.
3. AM Bagher. Comparison of LED and OLED. Sch. J. Eng. Tech., **2016**, 4(4), 206-210.
4. Paterson, L.; May, F.; Andrienko, D. Computer Aided Design of Stable and Efficient OLEDs. *J. Appl. Phys*. **2020**, 128, 160901.
5. Negi, S., Mittal, P. & Kumar, B. Impact of different layers on performance of OLED. *Microsyst Technol*. **2018***,* 24, 4981–4989J. Appl. Phys. 128, 160901 (2020)
6. Yu, J., Lou, S., Jiang, Y., Li, L., Li, Q., & Zhan, X. Novel hole blocking material for organic light-emitting devices. In *3rd International Symposium on Advanced Optical Manufacturing and Testing Technologies*: *Advanced Optical Manufacturing Technologies*. SPIE, **2007**, 6722, 374-378
7. Amruth, C., Pahlevani, M., & Welch, G. C. Organic light emitting diodes (OLEDs) with slot-die coated functional layers. *Materials Advances*. **2021**, 2(2), 628-645.
8. Nam, S., Kim, J. W., Bae, H. J., Maruyama, Y. M., Jeong, D., Kim, J., Kim, J. S., Son, W.-J., Jeong, H., Lee, J., Ihn, S.-G., Choi, H., Improved Efficiency and Lifetime of Deep-Blue Hyperfluorescent Organic Light-Emitting Diode using Pt(II) Complex as Phosphorescent Sensitizer. *Adv. Sci.* **2021**, 8, 2100586.
9. Hyein Ha., Young Jae Shim., Min Chul Suh,*: Highly Efficient Solution-Processed Organic Light-Emitting Diodes Containing a New Cross-linkable Hole Transport Material Blended with Commercial Hole Transport Materials, *ACS Appl. Mater. Interfaces* (**2021**), 21954–21963
10. Baldo, M. A., O'Brien, D. F., You, Y., Shoustikov, A., Sibley, S., Thompson, M. E., & Forrest, S. R. Highly efficient phosphorescent emission from organic electroluminescent devices. *Nature*. **1998**, 395(6698), 151-154.
11. Goushi, K., Yoshida, K., Sato, K., & Adachi, C. Organic light-emitting diodes employing efficient reverse intersystem crossing for triplet-to-singlet state conversion. *Nature Photonics*. **2012**, *6*(4), 253-258

12. Xiaofeng, Luo, et al. "Sterically wrapping of multi-resonant fluorophores: an effective strategy to suppress concentration quenching and spectral broadening." *Frontiers in Chemistry* 11 (**2023**): 1198404.
13. Gawale, Yogesh, et al. "Forthcoming hyperfluorescence display technology: relevant factors to achieve high-performance stable organic light emitting diodes." *Frontiers in Chemistry* 11 (**2023**): 1211345.
14. Zhu, Minrong, and Chuluo Yang. "Blue fluorescent emitters: design tactics and applications in organic light-emitting diodes." *Chemical Society Reviews* 42.12 (2013): 4963-4976. Micromachines **2019**, 10, 344
15. Song, Wook, and Jun Yeob Lee. "Degradation mechanism and lifetime improvement strategy for blue phosphorescent organic light-emitting diodes." *Advanced Optical Materials* 5.9 (**2017**): 1600901
16. Teng, Jin-Ming, Yin-Feng Wang, and Chuan-Feng Chen. "Recent progress of narrowband TADF emitters and their applications in OLEDs." *Journal of Materials Chemistry* C 8.33 (**2020**): 11340-11353.
17. Tao, Youtian, Chuluo Yang, and Jingui Qin. "Organic host materials for phosphorescent organic light-emitting diodes." *Chemical Society Reviews* 40.5 (**2011**): 2943-2970.
18. Park, Jong-Heum, and Trevor M. Penning. "Polyaromatic hydrocarbons." Process-induced food toxicants: *Occurrence, formation, mitigation, and health risks* (**2009**): 243-282.
19. Dabestani, Reza, and Ilia N. Ivanov. "A compilation of physical, spectroscopic and photophysical properties of polycyclic aromatic hydrocarbons." *Photochemistry and photobiology* 70.1 (**1999**): 10-34.
20. Tanaka, Hiroyuki, et al. "Hypsochromic shift of multiple-resonance-induced thermally activated delayed fluorescence by oxygen atom incorporation." *Angewandte Chemie International Edition* 60.33 (**2021**): 17910-17914.
21. Madayanad Suresh, Subeesh, et al. "A Deep-Blue-Emitting Heteroatom-Doped MR-TADF Nonacene for High-Performance Organic Light-Emitting Diodes. " *Angewandte Chemie* 135.8 (**2023**): e202215522.